RAS Techniques and Instruments

RASTI **5,** 1–16 (2026)
Advance Access publication 2026 March 18

https://doi.org/10.1093/rasti/rzag018

The Preliminary Mauve Science Programme: science themes identified for the first year of operations

Mauve Science Collaboration – Year 1: Marcel A. Agüeros [1], Don Dixon [2], Chuanfei Dong [3,4], Girish M. Duvvuri [2], Patrick F. Flanagan [5], Christopher M. Johns–Krull [6], Hongpeng Lu [3], Hiroyuki Maehara [7,8,9], Kosuke Namekata [7,8,10,11], Alejandro Núñez [1], Elena Pancino [12], Sharmila Rani [12], Anusha Ravikumar [13], T. A. A. Sigut [13], Keivan G. Stassun [2], Jamie J. Stewart [5], Krisztián Vida [14], Emma T. Whelan [5], Benjamin J. Wilcock [15], Sharafina Razin [15], Arianna Saba [15,16], Ian Stotesbury [15], Giovanna Tinetti [15,16], Marcell Tessenyi [15] and Jonathan Tennyson [15,17]★

[1]*Department of Astronomy, Columbia University, 550 West 120th Street, NY 10027, New York, USA*
[2]*Department of Physics and Astronomy, Vanderbilt University, Nashville, TN 37235, USA*
[3]*Department of Astronomy, Boston University, Boston, MA 02215, USA*
[4]*School of Natural Sciences, Institute for Advanced Study, Princeton, NJ 08540, USA*
[5]*Department of Physics, Maynooth University, Maynooth, Co Kildare, W23 F2H6, Ireland*
[6]*Department of Physics and Astronomy, Rice University, Brockman Hall for Physics Suite 201, 6100 Main Street, Houston, TX 77005, USA*
[7]*The Hakubi Center for Advanced Research, Kyoto University, Yoshida-Honmachi, Sakyo-ku, Kyoto 606-8501, Japan*
[8]*Department of Physics, Kyoto University, Kitashirakawa-Oiwake-cho, Sakyo-ku, Kyoto 606-8502, Japan*
[9]*Subaru Telescope Okayama Branch Office, National Astronomical Observatory of Japan, National Institutes of Natural Science, 2-21-1 Osawa, Mitaka, Tokyo 181-8588, Japan*
[10]*Heliophysics Science Division, NASA Goddard Space Flight Center, 8800 Greenbelt Road, Greenbelt, MD 20771, USA*
[11]*Department of Physics,The Catholic University of America, 620 Michigan Avenue, N.E. Washington, DC 20064, USA*
[12]*INAF – Osservatorio Astrofisico di Arcetri, Largo Enrico Fermi 5, I-50125 Firenze, Italy*
[13]*Department of Physics and Astronomy, Institute for Earth and Space Exploration, the University of Western Ontario, 1151 Richmond Street, London, Ontario N6A 3K7, Canada*
[14]*Konkoly Observatory, Konkoly-Thege Miklós út 15-17, Budapest 1121, Hungary*
[15]*Blue Skies Space Ltd, 69 Wilson Street, London EC2A 2BB, UK*
[16]*Department of Physics, King's College London, Strand, London WC2R 2LS, UK*
[17]*Department of Physics and Astronomy, University College London, Gower Street, WC1E 6BT London, UK*

Accepted 2026 March 3. Received 2026 March 1; in original form 2026 January 8

ABSTRACT

Mauve is a low-cost small satellite developed and operated by Blue Skies Space Ltd The payload features a 13 cm telescope connected with a fibre that feeds into a UV-Vis spectrometer. The detector covers the 200–700 nm range in a single shot, obtaining low resolution spectra at R∼20–65. Mauve has launched on 2025 November 28, reaching a 510 km Low-Earth Sun-synchronous orbit. The satellite will enable UV and visible observations of a variety of stellar objects in our Galaxy, filling the gaps in the ultraviolet space-based data. The researchers that have already joined the mission have defined the science themes, observational strategy, and targets that Mauve will observe in the first year of operations. To date 10 science themes have been developed by the Mauve science collaboration for year 1, with observational strategies that include both long duration monitoring and short cadence snapshots. Here, we describe these themes and the science that Mauve will undertake in its first year of operations.

Key words: Instrumentation – UV astronomy – spectrophotometry – stellar objects.

1 INTRODUCTION

The study of the universe through ultraviolet (UV) radiation has enabled many breakthroughs in the past decades. Space telescopes with UV capabilities, such as the International Ultraviolet Explorer (IUE) (A. Boggess et al. 1978), the *Hubble Space Telescope* (*HST*) and UVIT@Astrosat (A. Kumar et al. 2012), have provided decades of valuable astrophysical data. However, as these facilities have either been decommissioned or are highly oversubscribed, the UV region of the electromagnetic spectrum

★ E-mail: j.tennyson@ucl.ac.uk

Table 1. Mauve satellite technical specifications.

Item	Specification
Telescope	13 cm Cassegrain
Spectral range	200–700 nm
Spectral resolution	10.5 nm ($R = 20$–65)
Sky coverage	–46.4 to 31.8 deg (ICRS coord. ep=J2000)
Orbit	Sun-synchronous LEO, 510 km, LTDN 10:30
Pointing solution	High-performance star tracker and gyro

remains under-sampled, with existing data sets often fragmentary and infrequently acquired.

To address this gap, Blue Skies Space Ltd (BSSL) has developed Mauve, a small satellite, using high-heritage, off-the-shelf technology that covers a broad spectral range, simultaneously spanning the near-ultraviolet (NUV) and visible wavelengths.

Pioneering a new model for science satellites and space science (R. Archer et al. 2020), Mauve launched on 2025 November 28 and will begin a collaborative scientific programme in early 2026, that focuses on monitoring stellar activity and variability. A major strength of the Mauve science programme is the availability of thousands of observational hours each year for its consortium members. This makes it ideal for time-domain astronomy, where hundreds of hours can be dedicated to both, long-duration observations and repeat observations. Additionally, Mauve will be ideally placed to conduct pilot studies and high-risk investigations.

Providing constraints on stellar activity, variability, and the influence a host star has on its local environment and potential planet habitability are a few examples of the areas Mauve will contribute to over its three-year lifetime.

In this paper, we present an introduction to the core science themes developed by the Mauve Science Team. Section 2 introduces the specifications of the Mauve satellite, Section 3 presents the commissioning and calibration plans while Section 4 provides the breakdown of the science areas Mauve will cover.

2 PLATFORM AND PAYLOAD

The satellite, a 16U smallsat, designed and built by BSSL's industrial partners, C3S and ISISpace, houses a 13 cm Cassegrain telescope and two fibre-fed spectrometers for redundancy. Each spectrometer contains a CMOS linear array detector, covering the 200 to 700 nm range in a single exposure. Table 1 provides a breakdown of the technical specifications of the Mauve spacecraft and its payload. More details on the payload specification and assembly of the Mauve satellite can be found in Stotesbury et al. (in preparation).

As final operational performance will only be known post-commissioning, the BSSL team and the Mauve Science Team are considering multiple performance scenarios to prepare the science programme and optimize the observation schedule. MauveSim (A. Saba et al. 2025), an end-to-end simulator, was developed to assess the science capabilities of the satellite. The simulations presented here are derived from the most recent ground-based testing and expected in-orbit performance, with appropriate margins applied. The detector temperature, for instance, directly influences the thermally induced noise on the detector and the system's overall performance. Following commissioning, MauveSim will be revised and updated to reflect the final in-flight performance. Pending commissioning and final performance, some Mauve science themes may be updated to account for spacecraft in-orbit behaviour.

3 COMMISSIONING AND CALIBRATION

Mauve is equipped with a low-resolution spectrometer, resulting in each detector resolution element spanning approximately 40 pixels. This configuration leads to significant oversampling of the instrument line function – a matrix that describes photon energy redistribution i.e. the probability of detecting an incident photon at any given pixel. Due to this oversampling, each pixel collects photons from a range of wavelengths, making it impossible to determine the exact energy of a photon striking a specific pixel. Any observation obtained with Mauve can be represented as the matrix product of the true stellar spectrum, the telescope's effective area (ARF, representing total detector throughput), and the instrument line function (RMF). However, this matrix operation is non-reversible, meaning that the true stellar spectrum cannot be directly separated from the instrumental effects to recover the intrinsic stellar flux in physical units. Because all flux calibration information is contained within the ARF and RMF, calibrating Mauve involves adjusting these arrays such that the observed spectrum of a stable reference star with a well-known spectrum matches the simulated spectrum of the same source. When the observed and simulated spectra of the reference star match with each other, the calibration is deemed successful. If discrepancies remain, the ARF and RMF are iteratively refined until a satisfactory match is achieved. During the commissioning phase and routinely throughout nominal operations, BSSL will generate and update the calibration files required by users to perform accurate data analysis.

The pointing stability was simulated and modelled by ISISpace, but is a primary analysis of the commissioning stage. Prior to launch the relative pointing error (RPE) of the system was estimated to be approximately 12 arcsec across a 10 s window. This information has been incorporated into a pointing model for the system, enabling time-domain jitter analysis. Our estimates indicate that jitter-induced noise is negligible. The fibre diameter is 230 μm, corresponding to a half-cone FoV of approximately 47 arcsec.

A set of pre-defined standard calibration targets has been selected and will be observed periodically to monitor any variations in sensitivity and performance throughout Mauve's operational lifetime (Saba et al., in preparation). The current list of calibration targets includes bright, well-characterized, and photometrically stable stars, primarily A- and B-type stars that emit sufficient flux within the Mauve spectral range. These targets are chosen for their stability (they are non-pulsating and non-variable), high brightness in the Mauve band, ability to achieve a high signal-to-noise ratio (S/N) within seconds, and to avoid detector saturation during short exposures. Additionally, non-variable solar-type stars have been included among the calibration targets to improve calibration in the redder wavelengths.

To establish the initial post-launch pointing calibration, we selected Jupiter due to its exceptional brightness and large angular size. The planet enabled a first-order determination of the initial misalignment between the star tracker attitude solution and the telescope boresight. Subsequently, bright point sources (stars) were used to confirm and refine the misalignment identified from the Jupiter observations.

A comprehensive commissioning and calibration report will be released following Mauve's commissioning period, summarizing

the lessons learned during spacecraft commissioning and outlining the achievable calibration performance of the instrument. The commissioning phase is currently expected to last up to four months. However, BSSL will review this timeline with its industry partners and announce any schedule updates as needed.

4 THE MAUVE SCIENCE PROGRAMME

4.1 Mauve science planning

While BSSL is responsible for the development and operation of the satellite platform, as well as implementation of the observation schedule, the Mauve Survey Programme is designed as a collaborative, member-driven scientific initiative. Survey members contribute to the definition of science themes, objectives, target lists, and observational strategies through a structured planning process conducted in coordination with BSSL.

The programme is led by the Mauve Science Team, a consortium of scientists from institutions across Europe, Asia, and North America. The Science Team was established during the survey design phase, prior to Mauve launch, through a membership subscription model under which participating organizations joined the collaborative survey programme. Institutions that joined at this early stage also joined the Science Team and contributed to survey planning and prioritization activities.

The participating member institutions include:

(i) Boston University
(ii) Columbia University
(iii) INAF – Osservatorio Astrofisico di Arcetri
(iv) Konkoly Observatory
(v) Kyoto University
(vi) Maynooth University
(vii) National Astronomical Observatory of Japan
(viii) Rice University
(ix) Vanderbilt University
(x) Western University

Science planning is conducted on an annual cycle. The core science themes for Year 1 are now largely established, with observations scheduled to take place throughout 2026. However, the programme is dynamic and adaptable, and the Science Team will periodically review and update the observation schedule during the first year, incorporating new targets and refining strategies as needed.

Although the Year 1 Science Team has now been closed, new institutions and researchers are expected to join as members. These new members will have equal access to Mauve data and the opportunity to submit observation requests for the Mauve filler programme for year 1. Years two and three of the Mauve survey are still open, and planning for year 2 is expected to commence in April 2026.

In total, 5000 h have already been allocated to the collaborative Mauve Science Programme for Year 1, and distributed among the current themes. In addition, BSSL will retain a reserve pool of observing hours to accommodate performance margins, future requirements, and new science opportunities.

4.2 Science overview

Pre-flight constraints on the field of regard (FoR) limit Mauve observations to targets within the declination range of $+31.8^\circ$ to -46.4°; sources outside these bounds are currently inaccessible.

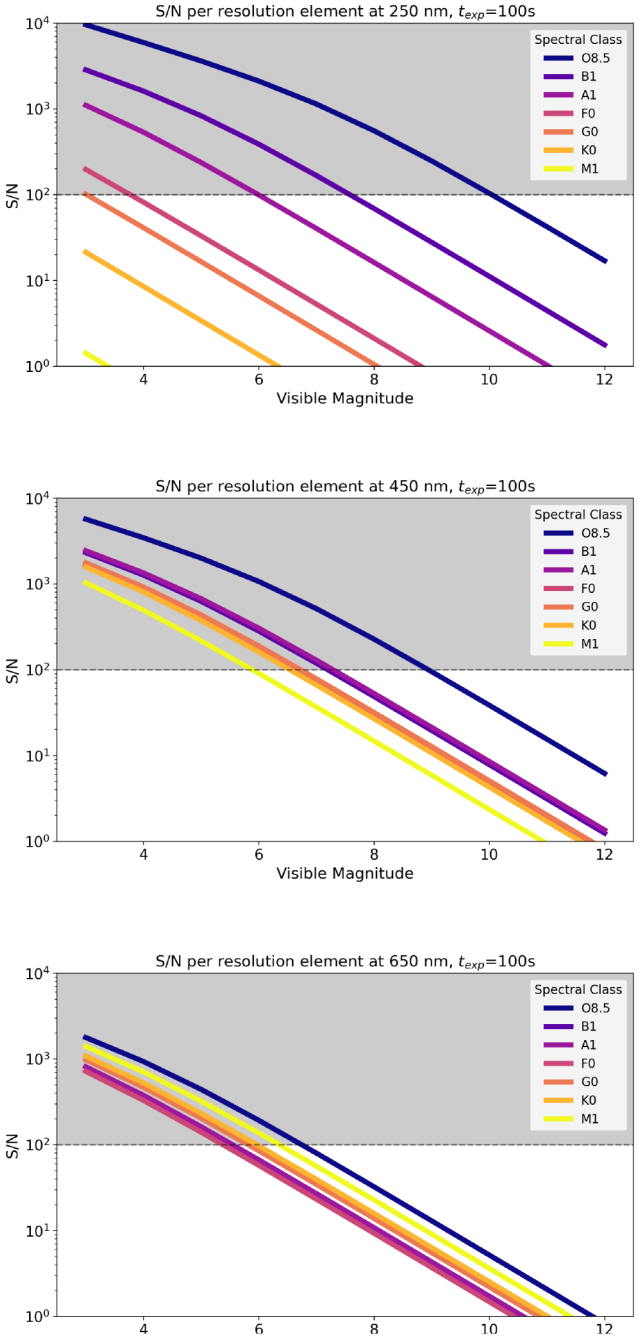

Figure 1. Expected Mauve S/N per resolution element (10.5 nm) at 250, 450, and 650 nm for a 100 s exposure time for different stellar types. The performance at the faint end is likely to be limited by the capacity of the spacecraft to track the target, which depends on factors such as stellar type and the presence of other sources in the field. Performance may also be constrained by systematics (e.g. noise saturation) at S/N per resolution element higher than 100. This is indicated in the plots as a shaded grey region above the dashed line.

In addition, pre-flight analyses were performed to estimate the telescope sensitivity limits and the corresponding target magnitude thresholds across different wavelength bands. The sensitivity plots in Fig. 1 show the expected signal-to-noise ratio (S/N) per 10.5 nm bin (one resolution element) as a function of visible magnitude for several wavelength bands. These predictions

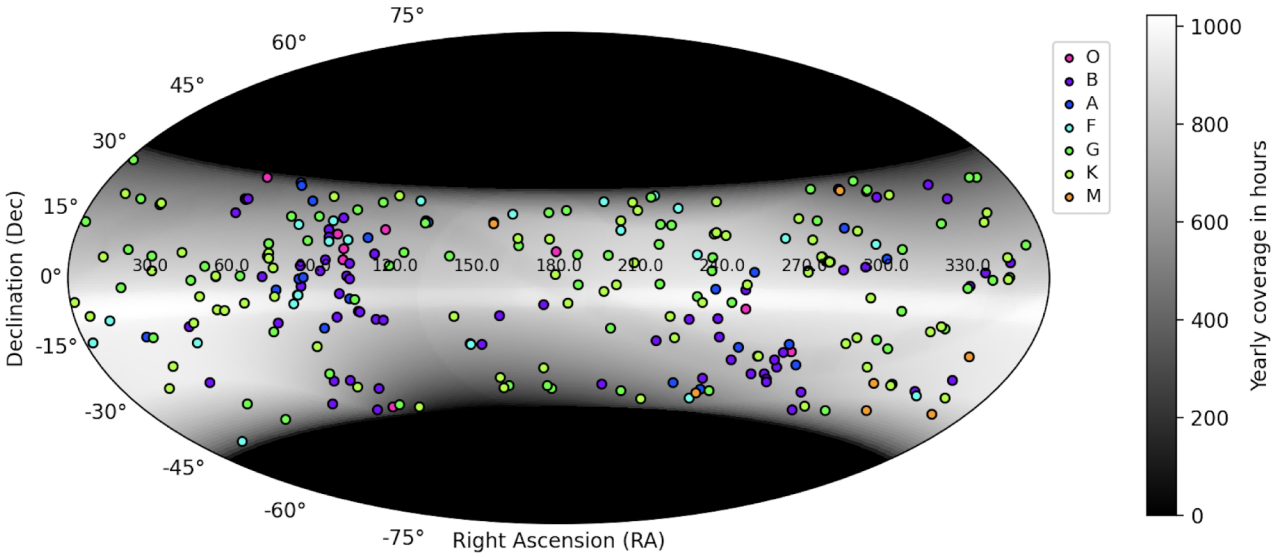

Figure 2. Candidate target list coloured by spectral type across the Mauve field of regard.

Table 2. Mauve science themes and corresponding observational programme types.

Science theme	Observational programme type
M-dwarf flares	Long-duration monitoring.
Superflares on young Sun-like stars	Long-duration monitoring.
Stellar CMEs	Long-duration monitoring.
Quiescent UV emission in low-mass stars	Short-cadence, single snapshots.
Future HWO targets	Short-cadence, single snapshots.
Young planet hosts	Short-cadence monitoring with repeats.
Classical Be star survey	Short-cadence, single snapshots.
Accretion variability (Herbig Ae/Be)	Short-cadence monitoring with repeats.
Dipper/Burster behaviour (Herbig Ae/Be)	Short-cadence monitoring with repeats.
Binaries in exotic populations	Short-cadence monitoring with repeats. Short-cadence, single snapshots.

are based on pre-launch performance models and ground-based characterization of the dark current noise (450 counts s^{-1}) and overall payload efficiency (see A. Saba et al. 2025). These sensitivity estimates are being progressively refined through ongoing commissioning activities and in-flight performance characterization. Updated sensitivity curves, reflecting the measured on-orbit performance of the instrument, will be released following completion of the commissioning and calibration phase.

An initial programme of 10 core science themes has been developed by the Science Team in the first year, with approximately 290 candidate stars identified by these themes (Fig. 2). Table 2 summarizes the science themes and the chosen observational strategy.

The selected science themes can be broadly categorized into the following research areas: stellar activity and variability, host-star/planet interaction, hot stars, and exotic populations in binaries. Specific themes can then also be grouped by three main observation strategies, i.e. long-duration monitoring programmes, short-cadence single snapshots, and short-cadence monitoring with repeats. These categories determine scheduling strategy and observation cadence. Long-duration monitoring (10–250 h) is typically focused on tracking stellar variability on specific targets over time. The themes using this observation strategy include studies of stellar activity and variability, specifically to understand the flare occurrence rates and to constrain the signatures of coronal mass ejections (CMEs) through flare-associated dimming.

The second category comprises short-cadence (<5 h) single snapshots, typically associated with large-scale statistical programmes observing many targets, or small groups of targets observed repeatedly. The themes related to short-cadence single-snapshot observations include investigations of exoplanet host stars and future Habitable Worlds Observatory (HWO) targets, the study of quiescent NUV emission in low-mass stars to constrain the evolution of rotation and magnetic activity in Sun-like (and lower mass) stars, and the classical Be star survey, designed to explore the mechanism that causes disc ejection.

Finally, the last observation strategy is short-cadence monitoring with repeat observations. These enable characterization and assessment of temporal evolution. The science themes that have adopted this observational strategy include young planet-host stars, accretion variability, and dipper/burster behaviour in Herbig Ae/Be stars, and studies of binary stars in exotic populations. These studies will elucidate the transition process from magnetic to non-magnetic accretion, and how key accretion and disc mechanisms evolve with increasing stellar mass in the context of star and planet formation. Additionally, Mauve will expand our understanding of binary evolution, revealing how a two-star system creates unique evolutionary pathways that are poorly understood.

4.3 Understanding Stellar variability and activity

Stellar flares and CMEs are energetic manifestations of stellar magnetic activity caused by the rapid and sudden release of magnetic energy via magnetic reconnection. In the case of the Sun, flares are sometimes accompanied by an increase in solar energetic particles, exhibiting a rapid increase in electromagnetic radiation from X-ray to radio; in some cases, they are also

accompanied by CMEs which release large amounts of plasma into space (K. Shibata & T. Magara 2011). While the impact of solar flares and CMEs on planetary space weather is well established (E. Kilpua, H. E. J. Koskinen & T. I. Pulkkinen 2017), studies of flares and CMEs for other stars and their impact on the planets orbiting around them remain underdeveloped. The goal of this science theme is to utilize Mauve's time-domain capabilities through long-duration monitoring of stars to study the impact of stellar variability and activity on a planet's chemistry and atmospheric escape. In addition, the short-cadence, single snapshots of low-mass stars will be utilized to quantify quiescent UV emission on low-mass stars. Through these observational strategies, these science themes aim to study the nature of NUV and optical continuum radiation from stellar flares on M-dwarfs and young G/K-dwarfs (Sun-like stars), probe stellar CMEs via ultraviolet (UV) dimming signatures, and constrain the evolution of rotation and magnetic activity in Sun-like and lower mass stars.

4.3.1 Radiation mechanisms of stellar flares on M-dwarfs and young Sun-like stars

The UV and X-ray radiation from stellar flares is thought to influence planetary atmospheres and surface environments, but its actual contribution is not well justified. Young Sun-like (G/K-type) stars, particularly those younger than ∼600 Myr, exhibit extremely active magnetic behaviour, producing 'superflares' with energies exceeding 10^{33} erg above their quiescent emission nearly daily, as revealed by *Kepler* and *TESS* observations (e.g. H. Maehara et al. 2012; K. Namekata et al. 2021). This suggests that such energetic flares on the early Sun could have significantly impacted atmospheric escape and chemistry on early Venus, Earth, and Mars when life may have first emerged. Likewise, exoplanets in the habitable zones of M dwarfs orbit very close to their host stars and may be subjected to repeated flare-driven UV irradiation, potentially altering their atmospheric chemistry (H. Chen et al. 2021). Thus, understanding the UV–optical continuum radiation of flares across stellar types is central to both exoplanetary habitability and early solar system evolution.

Despite its importance, the physical origin of the flare UV–optical continuum remains poorly understood. Many previous studies assumed an optically thick '10 000 K blackbody' continuum when estimating flare bolometric energies, but this assumption is based on limited observations of M-dwarf flares (S. L. Hawley & B. R. Pettersen 1991) and is unlikely universally valid. Solar flares frequently exhibit lower effective temperatures (K. Namekata et al. 2017), whereas some M-dwarf flares display much higher temperatures (∼20 000–30 000 K; W. S. Howard et al. 2020). Moreover, both solar and stellar flares sometimes show strong Balmer jump features and optical–UV continuum shapes indicative of optically thin or multitemperature components (A. F. Kowalski et al. 2013). Recent numerical models also suggest that optically thin radiation may be an origin of superflares on Sun-like stars (P. J. A. Simões et al. 2024). Because bolometric energy and UV flux estimates in *Kepler*/*TESS* studies depend directly on the assumed continuum model, any systematic deviation from the conventional blackbody assumption can lead to order-of-magnitude errors, profoundly affecting solar, stellar, and exoplanetary studies.

A unified understanding of the continuum radiation in both M-dwarf and young G/K-type stellar flares would therefore have wide-ranging implications. Improved UV flux estimates will refine atmospheric photochemistry and escape models for terrestrial exoplanets around M dwarfs. Re-assessing the UV output of the early Sun will advance our understanding of the atmospheric evolution of Venus, Earth, and Mars. Furthermore, identifying whether flare continuum emission arises from optically thin hydrogen recombination, optically thick Balmer/Paschen continua, or blackbody-like emission at high temperature will fundamentally revise our understanding of flare heating and radiative processes. These improvements will recalibrate the bolometric energies of the ∼millions of flares detected in *Kepler*/*TESS* light curves, providing a physically grounded interpretation for stellar activity across different spectral types. Within this broader context, the plan is to carry out UV monitoring observations for M-dwarf and young Sun-like stars.

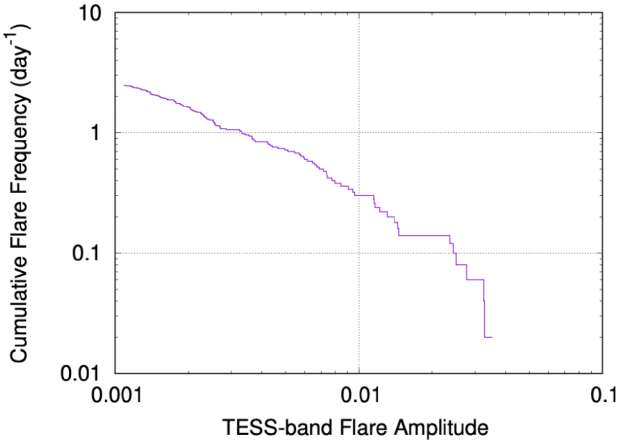

Figure 3. Cumulative flare frequency for AU Mic as a function of the flare amplitude in the *TESS* bandpass (600–1000 nm). The flare data are taken from K. Ikuta et al. (2023).

Objective 1: AU Mic presents a unique opportunity to characterize the continuum properties of M-dwarf flares. Thanks to Mauve's seamless 200–700 nm wavelength coverage, a time-resolved UV–optical spectra can be obtained. The cumulative flare frequency distribution of AU Mic derived from TESS Cycles 1 and 3 (Fig. 3; K. Ikuta et al. 2023) suggests that a 10-d observation should detect at least one flare with a *TESS*-band amplitude of ∼2.4 per cent and several events with amplitudes around 1 per cent. Since flares with amplitudes >0.1 per cent occur at a rate of ∼3 d^{-1} and typically last less than 30 min, over 90 per cent of time-resolved spectra will be obtained during quiescent periods. By summing more than 360 quiescent spectra (corresponding to >1800 s exposure), a high S/N pre-flare spectrum will be constructed to enable reliable flare-only spectral extraction.

Simulated Mauve spectra of a flare with a 300-s exposure indicate that, after binning over 40–80 pixels (10–20 Å), the blackbody continua with $T_{\rm eff}$=10 000 and 20 000 K can be distinguished. In addition, the difference in the simulated spectra for the blackbody continua $T_{\rm eff}$=10 000 and for the continua composed of *a* ∼10 000 K blackbody plus an optically thin Balmer-jump component with a Balmer jump ratio of ∼3 suggests that the NUV excess flux in the wavelength shorter than the Balmer limit (346.6 nm) due to the Balmer-jump component can be detectable with Mauve. See Fig. 4 for the model calculation. The minimum success criterion of this theme is to detect at least one flare and measure its effective temperature and Balmer jump ratio, while full success consists of detecting >3–4 flares and investigating the diversity of their NUV continua. If a superflare occurs by chance, Mauve's short exposure capability (30–60 s) will allow us to

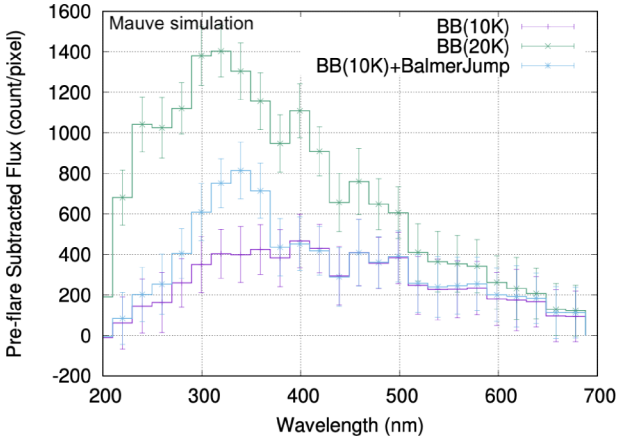

Figure 4. Comparison of simulated spectra based on different models for flare continuum. The flare amplitude for all models is 2.4 per cent in the *TESS* bandpass. The error bars represent three standard errors of mean for each bin.

resolve temporal changes in the continuum throughout the flare, providing unique constraints on the heating processes governing powerful M-dwarf flares.

Objective 2: Young Sun-like (G/K-type) stars such as V889 Her and ϵ Eridani offer an equally important window into the continuum properties of stellar superflares. These stars are rapid rotators with strong magnetic fields and produce frequent superflares with energies $\gtrsim 10^{34}$ erg. Although the associated brightening in the optical band is only ∼0.5–1 per cent, this does not reflect the total energetic output of the event. While cool stars have photospheric temperatures of roughly 3000–6000 K, the flare emission can be characterized by an effective temperature of ∼10 000 K (or higher). This naturally leads to a stronger relative enhancement at shorter wavelengths (UV and X-rays), while the optical contributes only a small fraction to the bolometric flare energy. The low optical contrast makes ground-based spectroscopic observations nearly impossible. *TESS* observations indicate that V889 Her flares of this scale occur every 1–2 d and last tens of minutes (K. Namekata et al. 2025). Simulations assuming a 1 per cent increase in flux relative to the quiescent emission ($\approx 2 \times 10^{34}$ erg) and a 5-min Mauve exposure show that spectra binned to 25–50 nm can distinguish optically thin continua – characterized by a pronounced Balmer jump – from 10 000 to 20 000 K blackbody continua. Thus, observations are planned for V889 Her for 100–380 h considering the high flare rate in *TESS*. ϵ Eridani shows only a modest flare rate in *TESS* photometry, yet *HST* FUV observations reveal that it produces flares far more frequently (R. O. P. Loyd et al. 2022). Although Mauve's sensitivity is more limited than that of *HST*, the largest flares detectable by Mauve are expected to occur roughly once or twice per day. Therefore, the plan is to conduct 50–100 h of observations of ϵ Eridani to capture these events.

As a goal, by combining Mauve observations with analytical continuum diagnostics (P. Heinzel 2024) and state-of-the-art 1D hydrodynamic models such as RADYN (K. Namekata et al. 2020; A. F. Kowalski, J. C. Allred & M. Carlsson 2024), the plasma temperature, column density, and the properties of non-thermal electron/proton beams responsible for heating will be inferred. These results will enable the construction of an observation-based spectral model for (super-)flares on M-dwarfs and Sun-like stars.

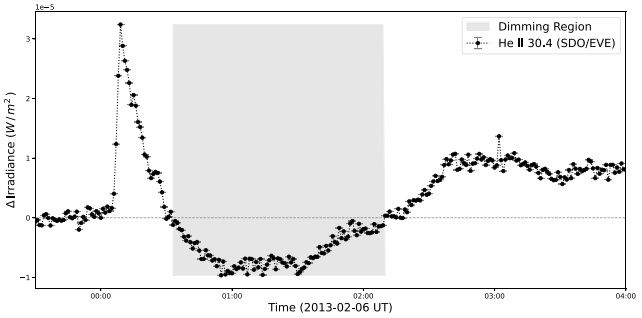

Figure 5. Post-flare coronal dimming associated with a CME detected in the Sun-as-a-star He II 30.4 nm line from SDO/EVE. The shaded region indicates the interval of CME-related dimming. While the He II line does not lie in the wavelength region covered by Mauve, the example illustrates that post-flare coronal dimming is associated with CME-related mass depletion. We expect analogous stellar coronal dimming events within the wavelength coverage of Mauve.

4.3.2 Probing coronal mass ejections through UV dimming signatures

In contrast to stellar flares, confirmed stellar CMEs beyond the Sun remain exceedingly rare due to the lack of spatially resolved diagnostics. A promising indirect method is the detection of flare-associated dimming signatures, analogous to solar coronal dimming. These dimmings may arise either from *emission dimming*, where plasma is evacuated from the stellar atmosphere, or from *obscuration dimming*, where cool filament or prominence material blocks background radiation (e.g. J. P. Mason et al. 2014; Y.-B. Chen et al. 2025).

A particularly valuable solar diagnostic is the He II 30.4 nm line, formed in the transition region at $\sim 5 \times 10^4$ K. Sun-as-a-star analyses with SDO/EVE and GOES/EUVS have shown that this line exhibits measurable obscuration dimmings during filament eruptions leading to CMEs (Y. Xu et al. 2024). Fig. 5 shows that, following an eruptive flare, the Sun-as-a-star (full-disc integrated) light curve of the He II 30.4 nm line exhibits a CME-associated dimming. This dimming corresponds to the transit of erupting filament material across the solar disc, which significantly attenuates the background emission. The amplitude and duration of this event demonstrate the sensitivity of transition-region diagnostics to CME-related obscuration and provide a benchmark for what could be detectable in stellar light curves. Beyond the transition region, dimming has also been observed in chromospheric diagnostics: for instance, Y. Jiang et al. (2007) reported Hα dimmings associated with filament eruptions, further supporting the notion that multiwavelength dimming phenomena are robust CME tracers across atmospheric layers. Together, these results reinforce the physical link between post-flare dimming signatures and CME mass budgets.

Building on this solar benchmark, Mauve's high-cadence spectrophotometry offers a unique opportunity to extend dimming-based CME detection to other stars. While the He II 30.4 nm line cannot be detected by Mauve, it is a suitable proxy for dimming tracers within stellar chromospheres. Several spectral diagnostics within Mauve's bandpass probe chromospheric and transition-region layers at 10^4–10^5 K, making them conceptually analogous to He II 30.4 nm (e.g. J. G. Doyle & A. Collier Cameron 1990; K. Namekata et al. 2021; A. M. Veronig et al. 2025). These include the Mg II h/k resonance lines (2796/2803 Å), the Ca II H&K lines (3934/3968 Å), and the Balmer series (e.g. Hα 6563 Å, Hβ 4861

Å). Each is sensitive to plasma density variations and obscuration by cool erupting material, with line cores expected to show the strongest dimming signatures. By monitoring these diagnostics after energetic flares, Mauve can search for persistent flux decreases beyond the flare's impulsive phase. The wavelength dependence and timing will make such signatures compelling indirect evidence of stellar CMEs.

Long-duration spectroscopic monitoring of active stars with high flare rates will be observed to ensure a statistically significant number of post-flare intervals during extended observing campaigns. By constructing Sun-as-a-star style light curves from Mauve spectra and applying solar-inspired analysis techniques, a systematic search for post-flare dimmings in Mg II, Ca II, and Balmer lines will be carried out. Detecting such signatures would provide strong evidence for CMEs on active stars.

4.3.3 Quiescent UV emission in low-mass stars

Observations of Sun-like stars throughout the 1960s showed that rotation and magnetic activity decrease over time at the same rate (A. Skumanich 1972), with the stars' spin-down thought to be due to angular momentum lost through magnetized winds. This coupling of rotation and the stellar magnetic field implies that observable indicators of the field's presence, such as optical emission lines or X-ray luminosity, also weaken over time.

However, the dependence of rotation or magnetic activity on age involves poorly understood physics, such as the magnetic field geometry and the degree of core–envelope coupling (e.g. V. Réville et al. 2015). Furthermore, theorists disagree on whether different magnetic activity indicators, which trace the heating of different atmospheric layers, should have a similar dependence on rotation. In short, many details remain unknown about how magnetic energy is distributed across stellar atmospheric layers and how that distribution changes as main-sequence stars age and spin down (B. Stelzer et al. 2013; B. Stelzer et al. 2016; T. Richey-Yowell et al. 2019).

To constrain the evolution of rotation and magnetic activity in Sun-like (and lower mass) stars, a sample of stars in open clusters with well-determined ages will be used (M. A. Agüeros et al. 2011, 2018; S. T. Douglas et al. 2014; A. Núñez & M. A. Agüeros 2016; A. Núñez et al. 2017, 2015, 2022, 2024; J. L. Curtis et al. 2019b, a, 2020). We will use Mauve to capture short-duration (i.e. minutes or hours) variability, typically associated with flares. Such flares will then be removed from our UV emission measurement to capture the quiescent level of emission.

This science theme will focus on the characterization of the transition region between the chromosphere and the corona as this hot, tenuous layer is where magnetically driven stellar UV emission originates, but how that emission varies as a function of mass, rotation, and age is poorly constrained observationally. The use of *GALEX* photometry data to study low-mass stars (e.g. K. Findeisen, L. Hillenbrand & D. Soderblom 2011; B. Stelzer et al. 2013; E. L. Shkolnik & T. S. Barman 2014; A. C. Schneider & E. L. Shkolnik 2018; T. Richey-Yowell et al. 2019), will be combined with Mauve's low-resolution UV spectrophotometry to greatly improve the ability to quantify quiescent UV emission, connect it with stellar rotation, and compare it to other indicators of magnetic activity. The primary objectives are:

(i) to compare UV fluxes among stars exhibiting different levels of magnetic activity, thereby identifying how UV output varies with stellar properties;

(ii) to evaluate the relationship between UV emission and chromospheric and coronal diagnostics, providing new insights into the influence of magnetic heating on stellar atmospheres;

(iii) to validate and extend trends suggested by *GALEX* photometry, while assessing the added value of Mauve's spectrophotometric coverage; and

(iv) to provide input for planetary atmosphere models to study their evolution and habitability properties.

The integrated UV fluxes over well-defined spectral bands will be extracted from the science-ready Mauve spectrophotometry. These measurements will be combined with existing catalogues of rotation periods, Hα equivalent widths, and X-ray luminosities to evaluate whether Mauve UV fluxes track established magnetic activity trends, and to identify any systematic departures from those trends. By comparing UV emission with chromospheric and coronal diagnostics, the aim is to understand how magnetic heating is partitioned across stellar atmospheric layers – and how UV flux can serve as a sensitive proxy for magnetic activity, especially in cases where optical or X-ray diagnostics are unavailable or ambiguous.

Mauve data of proposed targets will allow the exploration into how UV emission varies across late F and G stars with different activity levels, rotation rates, and ages. Furthermore, several of these targets also appear in the HWO Preliminary Input Catalogue (HPIC) (E. Mamajek & K. Stapelfeldt 2024). Although the focus is on the connection between rotation, activity, and age, these targets underscore the broader value of this work. Improving the understanding of the high-energy environments of solar-type stars is essential for interpreting future HWO observations of planetary systems and their atmospheres.

4.4 Exoplanet hosts

As explored in Section 4.3, UV/X-ray radiation from stellar flares could have a significant impact on the atmospheric escape and chemistry of the orbiting planets. In the case that these flares are accompanied by stellar CMEs, this can result in atmospheric erosion which further exposes the planets to stellar radiation (C. Kay, M. Opher & M. Kornbleuth 2016). Thus, understanding stellar magnetic activity and variability is crucial for assessing habitability in exoplanets (V. S. Airapetian et al. 2016).

In addition to long-duration studies providing insights into M-, G-, and K-type stars, Mauve has two science themes directly related to the study of exoplanet hosts that will be undertaken within Mauve's first year: the characterization of young planet hosts and early observations of HWO targets.

4.4.1 Young exoplanet hosts and HWO

Observations of young planet host stars serve two purposes: complementing transmission spectroscopy observations of the young planets by providing empirical spectra, and understanding how the evolution of stellar magnetic activity manifests in the NUV. The MUSCLES programme and its successors (K. France et al. 2016; A. Youngblood et al. 2021; D. J. Wilson et al. 2025) have produced panchromatic spectra of exoplanet hosts using *HST* for the UV wavelength regime and PHOENIX (P. H. Hauschildt 1993) models for the bulk optical and infrared (IR) emission. Stitching these two together has historically been a problem due to only some of the *HST* observations including data from 250 to 300 nm. Mauve can fill this gap with its spectral range and replace much

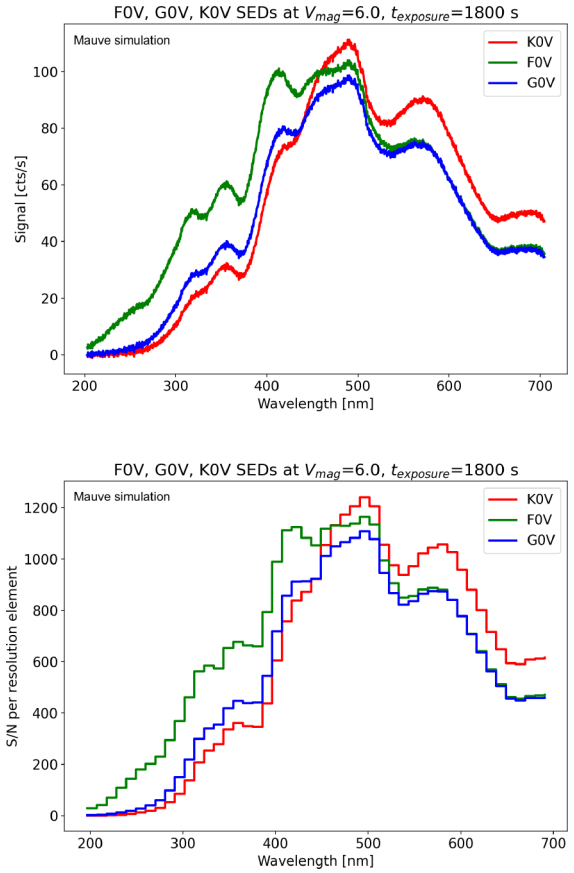

Figure 6. Simulated Mauve SEDs (upper panel) and S/N (lower panel) for example K0V, G0V, and F0V stars at $V_{\rm mag} = 6$ using an exposure time of 30 min.

of the optical portion of the spectral energy distribution (SED). Fig. 6 shows the expected Mauve SEDs and S/N per resolution element for example K0V, G0V, and F0V stars.

Besides enabling experiments for exoplanet theorists and providing constraints for exoplanet observers, the 200–300 nm range contains many transitions formed in the chromosphere, most notably Mg II lines. Stellar activity is often parametrized using a pair of power laws as a function of Rossby number with a transition point (A. D. Feinstein et al. 2024), but where this transition point is in stellar parameter space seems to be wavelength dependent (and not simply a product of different assumptions for calculating the Rossby number): coronal X-ray breakpoints seem earlier than far-ultraviolet (FUV) transition region lines or chromospheric Hα (J. S. Pineda, A. Youngblood & K. France 2021). Mg II forms across the upper chromosphere and extends at least partially to the transition region, so studying stellar activity in the NUV might pin down this wavelength dependence. The current candidate planet hosts span ages across 1–500 Myr, an interval that contains the breakpoints for most activity broken power-law relations.

The goal of this science theme would be to measure the UV spectra and variability of known young planet hosts, on short time-scales to verify whether the measurement is being affected by a flare, and on longer time-scales to account for potential activity cycle variation.

As part of the characterization of HWO targets theme, a sample of ∼40 targets has been identified within Mauve's FoR. These candidate targets have been selected from the priority A target list for the primary mission of the HWO, where they aim to directly image an Earth-sized planet in the liquid water zone of a star.

By providing visible to NUV spectrophotometry of these targets, Mauve can fill in gaps in the SEDs of these stars to inform HWO on mission design requirements, yield estimates, and contribute to a library of panchromatic spectrophotometry for main-sequence stars. The minimum requirement is to obtain a single snapshot of the NUV spectrum that can be published as a resource for any scientific investigation that requires the NUV spectrum of a main sequence star as an input, but the primary intended purpose is to provide the HWO Target Stars and Systems Working Group to inform the survey plan. One plausible scientific use for this library is to compare the obtained spectra to the various stellar atmosphere models in circulation, such as the PHOENIX models, to determine how they differ from ground truth data for different spectral types. Another is to inform planet atmosphere modelling codes that need NUV spectra as inputs for work on haze production, chemical disequilibrium, and biosignatures.

4.5 Classical Be and Herbig Ae/Be stars

4.5.1 The classical Be star survey

Classical Be (CBe) stars are upper main-sequence, B-type stars ($2.5 - 20\,{\rm M}_\odot$) that exhibit emission lines in their spectrum (most prominently Hα at $\lambda = 6562.8$ Å), an IR excess beyond 1 μm, and continuum polarization at the level of approximately 1 per cent (J. M. Porter & T. Rivinius 2003). The interpretation is that classical Be (CBe) stars are main-sequence B stars surrounded by a thin, gaseous, equatorial disc in which the emission lines and IR excess are formed by recombination in the disc gas (T. Rivinius, A. C. Carciofi & C. Martayan 2013). CBe stars are very common: it is estimated that perhaps one-fifth of all main-sequence B-type stars have been CBe stars at one time (J. Zorec & D. Briot 1997). The CBe stars are distinct from the more familiar Herbig Ae/Be stars in that CBe IR SEDs show no evidence for dust. While the Herbig Ae/Be stars are thought to be pre-main sequence objects still embedded in the remnants of their primordial accretion discs (L. B. F. M. Waters & C. Waelkens 1998), the discs of the CBe stars are thought to be *out-flowing, decretion discs* formed by mass ejected from the central stars (T. Rivinius et al. 2013).

The central mystery of the CBe stars is that the mechanism that causes the disc ejection is unknown despite decades of observations and modelling. Over the years, disc formation has been hypothesized to include one or more of the following: rapid stellar rotation, non-radial pulsation (NRP), magnetic fields, stellar winds, and binarity. Among this list, rapid stellar rotation has long been thought to play a key role, an idea dating back to O. Struve (1931). In this view, the CBe stars are postulated to rotate close to their critical (equatorial) rotation speed, defined as

$$V_{\rm crit} = \left(\frac{2GM_*}{3R_{\rm p}}\right)^{1/2}, \qquad (1)$$

where M_* is the stellar mass and $R_{\rm p}$ is the polar radius.[1] For a star rotating at its critical velocity, the effective gravitational acceleration at the equator vanishes and the material there effectively orbits the star. If a CBe star actually rotates with an

[1] At critical rotation, the equatorial radius is $R_e = (3/2)R_{\rm p}$ in the Roche approximation.

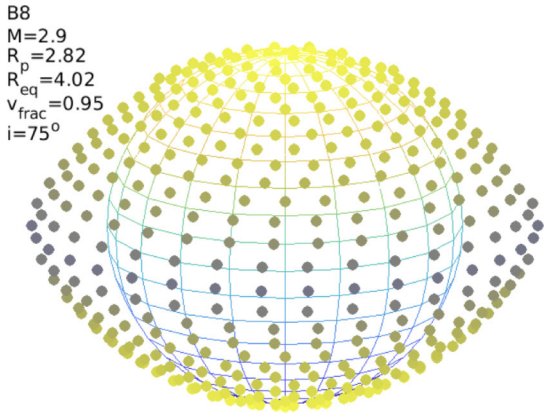

Figure 7. The distorted surface of a B8V star (mass 2.9 $M_\odot$, polar radius 2.82 $R_\odot$) rotating at 95 per cent of its critical velocity (363 km s^{-1}) seen at an inclination angle $i = 75^\circ$ ($i = 0^\circ$ corresponds to a star viewed pole-on). The coloured circles represent surface 'patches' that can be seen by a distant observer. Gravitational darkening is illustrated by the colour of each patch, ranging from bright yellow for the hot pole ($T_{\rm eff} = 13\,000$ K) to dark grey for the cooler equator ($T_{\rm eff} = 8000$ K). To compute the SED seen by a distant observer, the intensity for each surface patch is computed using local values of ($T_{\rm eff}$, log g), and then intensities for all patches are summed, weighted by their solid angles.

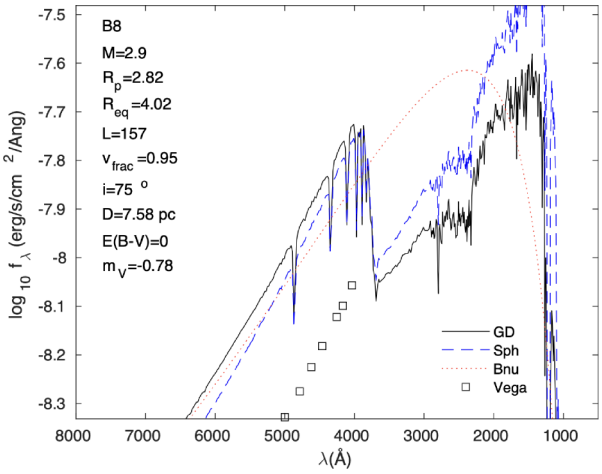

Figure 8. Simulated fluxes at the Earth for the B8V CBe star of Fig. 7 seen at a distance of 15 pc compute with the `Bedisk` (T. A. A. Sigut & C. E. Jones 2007) and `Beray` (T. A. A. Sigut 2018) codes. The solid black line is the predicted optical and NUV fluxes for gravitationally darkened, rotationally distorted star rotating at 95 per cent of its critical velocity seen at an inclination angle of $i = 75^\circ$. The dashed blue line gives the fluxes expected for a spherical, non-rotating star. The red dotted line is the prediction of a black body at the nominal (non-rotating) $T_{\rm eff}$, and the square symbols are the calibrated Vega fluxes from D. F. Gray (2021) included for reference.

equatorial speed of V_e, the parameter $v_{\rm frac} \equiv V_e/V_{\rm crit} \leq 1$ controls how effective rapid stellar rotation is in aiding disc ejection. Some postulated disc ejection mechanisms depend very strongly on the value of $v_{\rm frac}$. For example, a promising candidate is NRP (T. Rivinius, D. Baade & S. Štefl 2003), yet to be effective, NRP requires $v_{\rm frac}$ close to unity as it naturally produces flows with velocities on the order of the sound speed in the gas ($\approx$10 km s^{-1}); for these perturbations to result in the ejection of material, the star must be very near critical rotation.

Spectroscopic estimates of $v_{\rm frac}$ are complicated by the need for accurate stellar parameters and good measurements of $v \sin i$, the projected equatorial rotation velocity which can be deduced from the rotational broadening of spectral lines. For many years, measurements suggested $v_{\rm frac} \sim 0.8$, indicating that while the CBe stars are rapid rotators, they are not *critical rotators*. This conclusion was revised by R. H. D. Townsend, S. P. Owocki & I. D. Howarth (2004) who noted that gravitational darkening of the central B star due to rapid rotation can cause equatorial rotation speeds derived from $v \sin i$ measurements to be significantly underestimated. It has long been known that rapid stellar rotation leads to a distorted stellar surface and a latitude-dependent $T_{\rm eff}$ and log(g) (H. Zeipel 1924; F. Espinosa Lara & M. Rieutord 2011). For example, Fig. 7 shows a B8V star rotating at 95 per cent of its critical rotational speed. The latitude-dependent $T_{\rm eff}$ is particularly important as for $v_{\rm frac} \approx 1$, the local $T_{\rm eff}$ at the equator becomes significantly cooler, and thus the most rapidly rotating portion of the stellar surface has its contribution to the overall spectrum diminished, with $v \sin i$ correspondingly underestimated. Despite initial enthusiasm for this idea (T. Rivinius et al. 2013), subsequent detailed modelling of the optical spectra of CBe stars including gravitational darkening has not established that the CBe stars as a group are critically rotating. Based on a sample of 233 CBe stars, J. Zorec et al. (2016) found $< v_{\rm frac} > \approx 0.8$ with the distribution characterized by the very wide range $0.35 \leq v_{\rm frac} \leq 0.95$, implying that much more energetic mechanisms are often required for disc ejection. Such mechanisms could potentially involve magnetic fields (L. A. Balona & D. Ozuyar 2021)[2] or binarity (B. Hastings et al. 2021).

Despite this picture, there still is hope for the critical rotation hypothesis. One significant omission in all of the analyses above is the neglect of the circumstellar disc in the modelling of the CBe SED and in the extraction of the $v \sin i$ estimates. In addition, all of this work is based upon ground-based, optical spectra. Access to space-based SEDs for the CBe stars opens the possibility of determining $v_{\rm frac}$ directly from the influence of gravitational darkening on the central star's NUV SED.

The goal of this science theme is to determine if the UV portion of late-type CBe stellar SEDs is consistent with the $v_{\rm frac}$ values obtained from optical spectra, or if the $v_{\rm frac}$ values need to be revised. This is a sensitive test of the models because the UV portion of the spectrum is much more sensitive to the temperature variations across the stellar surface caused by gravitational darkening. For late-type CBe stars, spectral types B4 and later, the NUV fluxes accessible by Mauve are shortward of the Rayleigh-Jean's blackbody tail and hence are very sensitive to variations in the local $T_{\rm eff}$ across the stellar surface. This is illustrated in Fig. 8 where the flux at the Earth is simulated for the rapidly rotating CBe star of Fig. 7. An example of the expected Mauve signal seen for the same star in Fig. 7 is shown in Fig. 9. Here, the optical and NUV SEDs, convolved to a resolution of $\lambda/\Delta\lambda = 50$, are shown for various rotational speeds ranging from $v_{\rm frac} = 0.50$ to 0.95. Shown are relative fluxes, all normalized to unity at $\lambda = 6000$ Å. Interstellar reddening, $E(B–V)$, was assumed to be zero, although the modelling can account for interstellar reddening following E. L. Fitzpatrick (1999).

This survey aims to use Mauve to observe a sample of about 65 CBe stars of spectral type B4 or later. These targets were selected

[2]There are currently no detections of magnetic fields in CBe stars, despite large survey searches.

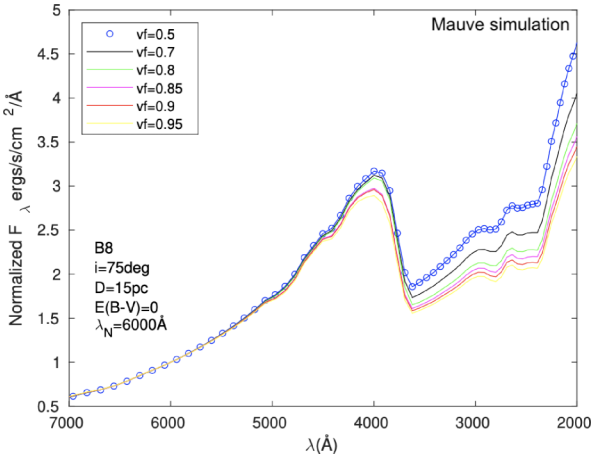

Figure 9. Predicted SEDs for the star of Fig. 7 as a function of the stellar rotation rate $v_{\rm frac}$ (see legend). The SEDs have been convolved to the same resolution as Mauve ($R = 50$) and are normalized to unity at $\lambda = 6000$ Å.

from the list of CBe stars from J. Zorec et al. (2016), all of which have estimates of $v_{\rm frac}$ based on optical spectra. The filtering was done for Mauve sky visibility and the B4 spectral type limit. Each target has estimated stellar parameters (M, $R_{\rm p}$, L) and $v_{\rm frac}$ from J. Zorec et al. (2016) which can be coupled with the system viewing inclination from T. A. A. Sigut & N. R. Ghafourian (2023), and the object's known distance and reddening, to produce a simulated SED in absolute flux units, similar to the example given in Fig. 8.

In addition to the selected CBe stars, five classical Ae (CAe) stars will be observed: CAe stars are thought to be the cool extension of the CBe phenomena to the cooler, A-type spectral class (see R. Anusha & T. A. A. Sigut 2025, and references therein). These objects are rarer, and hence fainter, than the CBe stars, yet their out-flowing discs are also thought to be driven by rapid stellar rotation (R. Anusha et al. 2021), and their SEDs may reveal this in the same way as described above for the CBe stars.

4.5.2 Variability of Herbig Ae/Be stars and implications for accretion and planet formation

Herbig Ae/Be stars are an important class of young stellar objects (YSOs), as they bridge the gap between solar-type stars like our Sun and massive, early-type stars (S. D. Brittain et al. 2023). They are considered the higher-mass counterparts of the classical T Tauri stars (CTTSs), representing a key transitional phase in stellar evolution. Typically aged between 2 and 8 Myr, Herbig Ae/Be stars are intermediate-mass (∼2–8 $M_\odot$) objects that continue to accrete material from their circumstellar discs. These stars remain surrounded by gas and dust, and exhibit a variety of observational signatures indicative of ongoing accretion and outflow activity and planet formation. While the formation and accretion processes of low-mass stars are comparatively well understood, and the earliest stages of planet formation in their discs much investigated, the picture becomes less clear for higher mass young stars. The magnetospheric accretion model, where the stellar magnetic field truncates the inner disc and channels infalling material along field lines, is well supported for CTTSs, but its applicability to Herbig Ae/Be stars remains uncertain. A key difference lies in the magnetic properties of these systems: whereas essentially all T Tauri stars possess strong magnetic fields (C. M. Johns-Krull 2007; C. Flores et al. 2022), only about 10 per cent

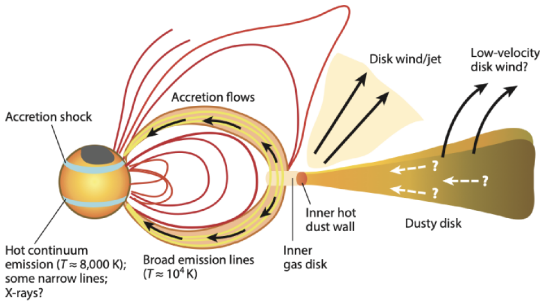

Figure 10. From L. Hartmann, G. Herczeg & N. Calvet (2016). The close circumstellar environment of a classical T Tauri star (CTTS). Strong stellar fields truncate the accretion disc near the co-rotation radius, directing accreting material along the field lines where bright accretion shocks form.

of Herbig Ae/Be stars show detectable magnetic fields (M. Reiter et al. 2018), and even these are substantially weaker. This low detection rate may reflect either genuinely weaker fields or more complex magnetic geometries that are difficult to measure with current techniques (S. D. Brittain et al. 2023). Consequently, the mechanism by which accretion proceeds in Herbig Ae/Be stars likely differs from the well-established magnetically controlled regime seen in CTTSs. A further difference between CTTSs and Herbig Ae/Be stars is that planet formation around Herbig Ae/Be stars likely begins earlier and proceeds faster due to their more massive and warmer but shorter lived discs (J. P. Williams & L. A. Cieza 2011).

This Mauve observing programme is designed to address these open questions through two complementary goals:

(i) To explore accretion physics in the intermediate-mass regime of Herbig Ae/Be stars, testing how the transition from magnetic to potentially non-magnetic accretion occurs.

(ii) To determine whether Herbig Ae/Be stars exhibit periodic brightness variations analogous to the 'dipper' and 'burster' behaviour seen in CTTSs, and to study if this is linked to early planet formation.

(i) Investigating accretion physics in Herbig Ae/Be stars

Monitoring the spectrophotometric modulation of light curves provides a powerful diagnostic of accretion in young stars, as variability often reflects changes in the accretion geometry or rate. Variability studies are therefore an excellent tool for probing accretion physics across stellar masses. For CTTSs, it is well established that accretion from the circumstellar disc to the stellar surface is regulated by a strong magnetic field (Fig. 10), which truncates the disc at approximately five stellar radii above the surface (N. Calvet & E. Gullbring 1998). Material follows magnetic field lines onto the star, impacting in compact regions – accretion 'footpoints' – that cover a small fraction of the stellar surface. If the stellar dipole is misaligned with the rotation axis, or if higher order field components dominate (S. G. Gregory & J. F. Donati 2011), the footpoints become localized, producing rotationally modulated photometric variability as they move in and out of view (L. M. Rebull et al. 2020). However, if the magnetic field is weak or absent, as is thought to be the case for most Herbig Ae/Be stars, the situation changes drastically. Extrapolating the field geometry inward suggests that accretion could occur over a much larger area of the stellar surface, potentially forming an equatorial

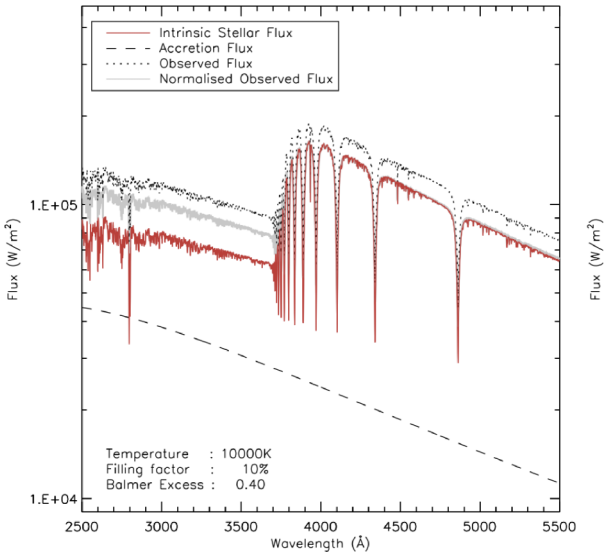

Figure 11. From J. R. Fairlamb et al. (2015). The red spectrum is an A0 photosphere and the black dashed line shows the accretion flux. These sum to produce the observed black dotted spectrum, which when renormalized to match the photospheric (red) spectrum longward of the Balmer jump produces the light grey spectrum showing a substantial excess shortward of the Balmer jump.

accretion ring in the limit of negligible magnetic confinement. In this scenario, the accretion emission would show weak or no rotational modulation, an important observational signature that Mauve is well equipped to detect. The continuum emission from accretion shocks in CTTSs typically has a temperature of around 10 000 K (J. A. Valenti, G. Basri & C. M. Johns 1993), similar to the effective temperature of an A0 star. At first glance, this similarity might make accretion emission in Herbig Ae/Be stars difficult to detect. However, J. R. Fairlamb et al. (2015) demonstrated that the accretion excess remains clearly visible in the spectral region shortward of the Balmer jump, providing a reliable diagnostic for accretion even in these hotter stars (Fig. 11). Mauve is particularly well suited to study this phenomenon across a large number of targets. Simulations using MauveSim (A. Saba et al. 2025) for the Herbig Ae star AB Aur ($V = 7.05$) show that in a 300-s exposure, the accretion excess shortward of the Balmer jump is readily detectable. In Fig. 12 the expected photospheric emission of the A0 star (shown in orange in the simulation) contrasts clearly with the purple excess due to accretion. By monitoring the variability of this excess emission over time, we can directly probe in the accretion rate and geometry in Herbig Ae/Be stars. In addition to the blue continuum, accretion also produces strong hydrogen recombination emission lines, particularly Hα and other Balmer lines, as gas flows along magnetic channels or accretes directly from the disc. Although Mauve's low spectral resolution will broaden these lines as shown in Fig. 13, flux variations in Hα remain a sensitive and independent tracer of accretion variability. Combining line and continuum diagnostics will provide a comprehensive picture of the accretion processes in these intermediate-mass stars.

(ii) Do Herbig Ae/Be stars exhibit dipper and burster behaviour?

The relationship between star and planet formation is investigated by targeting several key properties in YSOs. These are accretion–ejection connection, variability, and accretion disc

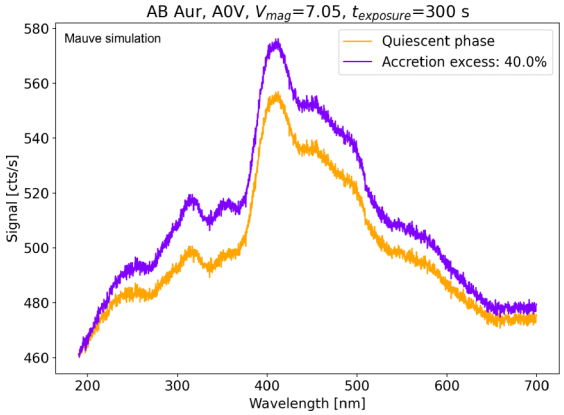

Figure 12. Simulated observed spectrum of AB Aur using MauveSim. Input spectrum is a star of the same spectral type (HD 143459) scaled to the V magnitude of AB Aur. Drawn in purple is how the accretion excess is expected to change the slope of the emission, specifically shortward of the Balmer jump (e.g. J. R. Fairlamb et al. 2015).

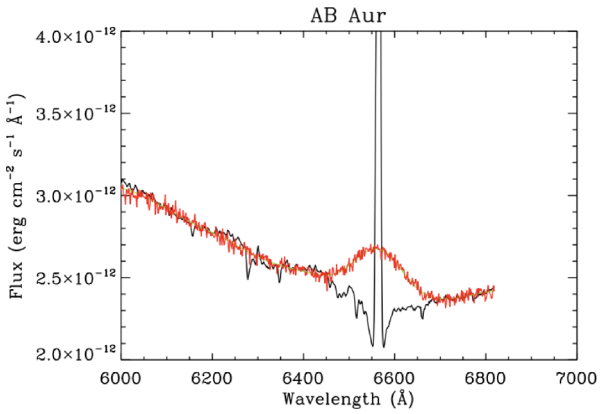

Figure 13. A spectrum of AB Aur in the neighbourhood of the Hα line taken at a resolution of ∼1000 shown in black. This same spectrum convolved to the resolution of Mauve is shown in green and that spectrum observed at signal-to-noise ratio (SNR) = 100 is shown in red.

structure (C. Pinte et al. 2023; I. Pascucci et al. 2023; W. J. Fischer et al. 2023). Accretion–ejection connection and variability have primarily been observed at optical and IR wavelengths (E. T. Whelan et al. 2014; A. M. Cody et al. 2017), while submillimetre observations have revealed the structure of discs in amazing detail (S. M. Andrews et al. 2018). The link between accretion and outflows is relevant to how planets form as outflows launched from the accretion discs are theorized to remove angular momentum thus driving accretion and disc evolution and shaping the initial conditions for planet formation (I. Pascucci et al. 2025). This activity is studied by targeting key emission lines in high-spectral and spatial resolution data allowing the mass accretion rate to be derived, and the kinematics, morphology, and physical conditions in the outflows to be mapped and accretion and outflow activity linked (A. Kirwan et al. 2022; M. Birney et al. 2024). Variability in the dynamical processes within the system, such as accretion onto the star, further impacts on properties of the accretion discs and thus the initial conditions for planet formation (L. A. Cieza et al. 2016; I. Das, E. Vorobyov & S. Basu 2025). Stellar variability can also point to activity in the inner disc associated with planet formation (P. P. Petrov et al. 2015; M. Koutoulaki

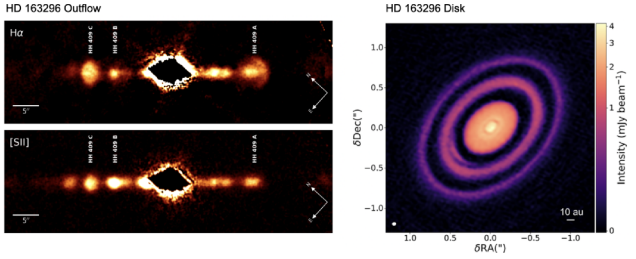

Figure 14. Left: VLT/MUSE observations of the bipolar jet driven by the Herbig Ae/Be star HD 163 296 taken from A. Kirwan et al. (2022). Right: Map of the HD 163 296 disc recorded in the 1.25 mm continuum taken from A. Isella et al. (2018). The dust rings and substructures are interpreted as evidence that planet formation processes are active in the disc.

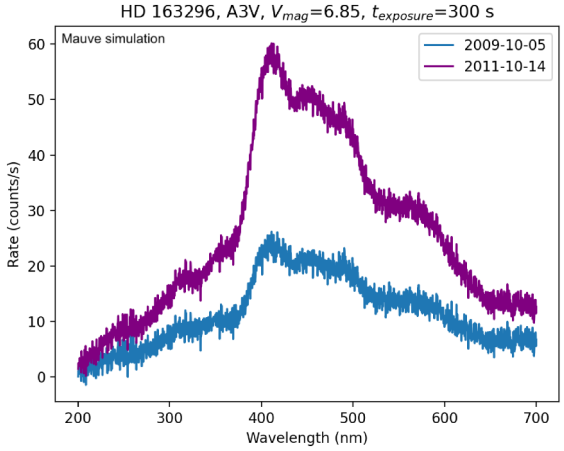

Figure 15. Simulated Mauve spectra of HD 163296, a Herbig Ae star with $V_{\rm mag} = 6.85$. The simulations are based on two epochs of X-Shooter observations that exhibit pronounced temporal variability. The noise levels in the simulated Mauve spectra correspond to an exposure time of 300 s.

et al. 2019). Finally, high angular resolution observations of the discs can reveal structure caused by orbiting planets or indeed in rare cases the protoplanets (S. M. Andrews et al. 2018; R. F. Capelleveen et al. 2025).

Low mass YSOs are known to exhibit variability over a range of time-scales (W. J. Fischer et al. 2023) and dipper and burster behaviour has attracted much study (R. Bonito et al. 2023). Dipper and burster behaviour refers to specific types of variability which last for days and are often linked to accretion and inner disc activity (A. M. Cody et al. 2014). Dippers experience periodic drops in brightness, which are thought to occur when material from their circumstellar disc intermittently blocks the star's light (P. P. Petrov et al. 2015). This can be caused by the misalignment of the disc or the presence of large, dense structures within it, such as dust clumps or gas streams (A. Empey et al. 2025). Such structures occur during early planet formation. Bursters, on the other hand, exhibit sudden and dramatic increases in brightness, typically due to rapid, episodic accretion events where large amounts of material fall onto the star's surface [also see (i) above]. Although dipper and burster behaviour has most often been investigated in CTTSs, its implications for planet formation argue for systematic studies across a wider mass range.

Mauve will be used to construct light curves for a sample of Herbig Ae/Be stars to search for dipper and burster behaviour in the UV. As described above Herbig Ae/Be stars are strong accretors and they are also are associated with outflows, as seen in Fig. 14 (A. Kirwan et al. 2022). They are known to be variable, exhibiting photometric and spectroscopic changes on time-scales ranging from hours to months, and longer (I. Mendigutía et al. 2011) and they may have a lower incident of dipper behaviours (A. M. Cody et al. 2025). Also, the gas and dust in their circumstellar discs has been spatially resolved with unprecedented detail with ALMA, revealing Keplerian discs that show convincing evidence for the presence of forming planets (L. M. Stapper et al. 2022). Therefore, they are ideal targets for investigating the connection between variability, and planet formation processes at higher masses. The focus with Mauve will mainly be on sources that drive outflows and/or exhibit signs of ongoing planet formation within their discs. Particularly interesting targets will then be examined in greater detail using existing and forthcoming ESO VLT UVES and MUSE data. Fig. 15 presents simulated Mauve spectra based on two X-Shooter observations of the Herbig Ae star HD 163 296 ($V_{\rm mag} = 6.85$), illustrating the variability between epochs. Mauve will monitor HD 163 296 and similar sources with a typical cadence of 1–3 observations per day over time-scales ranging from 40 to 80 d.

4.6 Binaries in exotic stellar populations

A significant number of stars in the galaxy are formed in binaries or multiple systems, which give rise to complex interactions happening among the stars. Stars in such systems have thus different evolutionary trajectories compared to genuine single stars. These interactions lead to the formation of what are generally called exotic or non-canonical stellar populations, such as blue straggler stars (BSSs), yellow straggler stars (YSSs), red straggler stars (RSSs), sub-subgiants (SSGs), subdwarfs (sdB, sdO), Li-rich stars, and so on. The exact origin of each of these types of stellar exotica is still wrapped in mystery.

One of the intriguing products of stellar interactions are BSSs, which appear brighter and bluer (hotter) than the normal turn-off stars, lying along an extension of the main sequence in the optical colour-magnitude diagram (CMD). In spite of the numerous photometric and spectroscopic studies on BSSs, their origin and evolution are still debated (H. M. J. Boffin, G. Carraro & G. Beccari 2015). To date, two leading formation channels suggested to account for their formation in clusters are: mass transfer in binaries (W. H. McCrea 1964) and stellar collisions or mergers (J. G. Hills & C. A. Day 1976). Observational studies of BSSs suggest that a combination of all the formation channels is prevalent, but their importance varies based on many factors, including the stellar density of their host environments. Most BSSs in low-density environments such as open clusters are found in binaries, with approximately 76 per cent in NGC 188 with a range of orbital periods and eccentricities (R. D. Mathieu & A. M. Geller 2009). BSSs resulting from binary mass transfer usually have close companions, typically compact objects such as white dwarfs, unless the binary system was disrupted by supernova kicks. On the other hand, BSSs formed through mergers, either from stellar collisions or binary mergers, typically do not have close companions. If these mergers occur within triple or higher order multiple systems, the resulting BSS can have a companion (I. Iben & A. V. Tutukov 1999; H. B. Perets & D. C. Fabrycky 2009). Several observational studies of BSSs in the field and open clusters have detected white dwarf companions to them, implying that mass

transfer may be a likely formation route (N. M. Gosnell et al. 2014, 2015, 2019; N. Sindhu et al. 2019; A. Panthi et al. 2023). BSSs are thought to form via mass transfer occurring during different evolutionary phases, classified as case A, B, or C. These phases refer to the onset of mass transfer during the main sequence, before core helium burning, or after the exhaustion of core helium in the donor star (R. Kippenhahn & A. Weigert 1967; D. Lauterborn 1970).

Other class of UV-bright stars are sub-dwarfs that are hot (O and B type) stars, mostly burning helium in their core ($0.5\,M_{\odot}$) (U. Heber 2009, 2016). They are hotter and more compact than canonical helium-burning stars, where a mix of stellar evolutionary processes, mass loss, binarity, and maybe mergers play a major role, which is demonstrated by the existence of several subclasses among subdwarfs. A large amount of mass-loss, required to form subdwarfs at the point of He burning, is difficult to explain in the context of single-star evolution and remains a missing piece of puzzle in stellar evolution theory (H. Dawson et al. 2024). A large fraction of field sdB stars are found in close binaries with white dwarf or very low-mass main-sequence companions, which must have gone through a common-envelope phase of evolution.

Another anomalous class of exotic stellar populations that defy canonical single stellar evolution are SSGs, which lie on the redder side of the main sequence and are fainter than the normal sub-giants in an optical CMD (see N. Sindhu, A. Subramaniam & C. A. Radha 2018 and references therein). Most of the SSGs found in the field are in binaries and are chromospherically active; they are thought to be stars that are presently losing mass to an unseen companion (A. M. Geller et al. 2017). Finally, Li-rich stars are a rare class of evolved stars that exhibit an abnormally high abundance of lithium in their atmospheres (G. Wallerstein & C. Sneden 1982). They are observed at all evolutionary phases and their origin is still unclear. Among the various possible explanations in the literature, there are two different ideas involving a binary origin for the lithium enhancement, either mass transfer from an AGB star or a companion spinning up the visible star, thereby enhancing the lithium content on its surface (I. J. Sackmann & A. I. Boothroyd 1999; A. R. Casey et al. 2019).

From the observational perspective, high-quality photometric and spectroscopic data are crucial for accurately determining the properties of exotic stars and discerning their formation mechanisms. Therefore, UV imaging and spectroscopy offer a unique window to identify hot companions to the above-mentioned stars if present, thereby helping to constrain their formation and differences, if any, between the field and clusters populations. The NUV spectra will complement the existing spectra in visible wavelengths to estimate stellar parameters (L, $T_{\rm eff}$, R) using multiwavelength SEDs, test evolutionary models, and derive the properties of binary components if present. The other advantage of observing in UV is the large amplitude variations compared to optical and IR regimes in the case of pulsating stars, and stars exhibiting any kind of stellar activity. UV spectra will also enable the discernment of the evolutionary pathways of hot stars in the field and compare their properties with those in star clusters.

Three main pieces of evidence will be used in the search and characterization of binaries; specifically:

(i) Any UV excess which might indicate the presence of a hot companion. Our candidates are mostly low-mass ($<2\,M_{\rm sun}$) stars in various evolutionary phases, like main sequence, subgiant branch, red giant branch, hot subdwarfs. The hot companions are expected to be mostly white dwarfs or extremely low mass stars, with masses mostly in the range 0.1 to 0.5 $M_{\rm sun}$, thus we will be finding mostly unequal mass binaries.

(ii) Flux variability will be studied to determine if there are Keplerian motions (eclipses). Eclipses will be easier to find for close binaries which, depending on the radius of the brighter star, will be on orbits that can range from one to several hundred days. However, shorter periods below about 10 d will be disproportionally more likely to produce eclipses.

(iii) Activity indicators will be used to disentangle stellar activity from Keplerian motions. Activity can be a natural result of the stellar properties, such as for example for low mass main-sequence stars, but can also be stimulated by close binary interactions. To distinguish between the two, we will use the whole target list, including low-mass stars from other themes in a collaborative effort, to establish the baseline of 'normal' activity for different types of stars.

Mauve will be particularly useful in this respect for the first point, because it covers the NUV spectral region, for the second point because it will be possible to dedicate a sufficient amount of time to monitor each star, and for the third point because of the wide range of wavelengths covered, including many of the typical activity indicators (such as Ca H&K, NaD, Hα) and even some (like Mg II) which are not visible from the ground. While Mauve cannot resolve these lines due to its low resolution, light-curve data across these wavelengths can still be used to detect variability. Moreover, when variability is detected, the comparison of the red and blue UV variability will allow us to separate activity and pulsations (which change with passbands and thus colours) from Keplerian motions.

The three observables indicated above will later be combined with existing literature information and/or follow-up observations, including spectral time-series. For example, by combining spectral time-series with Mauve light curves, we will be able to determine all orbital parameters, including the masses of the binary components, which are crucial to perform stellar evolution computations and reconstruct the paths of formation for these stars. Additionally, literature or follow-up information about the chemical composition of the star will provide further clues on the evolutionary stage of the companion during mass transfer, if any.

5 DISCUSSION AND CONCLUSIONS

In this paper we have presented the science themes prioritized by the Mauve Science Team for the first year of Mauve's operations. Initial simulations with MauveSim suggest strong performance across the different scientific goals and observational approaches presented here. However, the actual performance of Mauve will be confirmed through in-orbit testing and calibration therefore as the mission evolves, Mauve's scientific focus and observational strategy will need to remain flexible. New members are expected to join the survey collaboration throughout Year 1, with additional observational hours released periodically. Future science themes may focus on the detailed characterization of accretion signatures in young, low-mass stars, as illustrated by the simulation in Fig. 16. Future publications will expand on Mauve's science operations, data analysis, satellite performances, and science results, including reporting on payload and detector ageing throughout the mission lifetime.

Further into the future, Mauve^{+} is part of a BSSL roadmap to deliver more performing UV satellites for astronomy compared

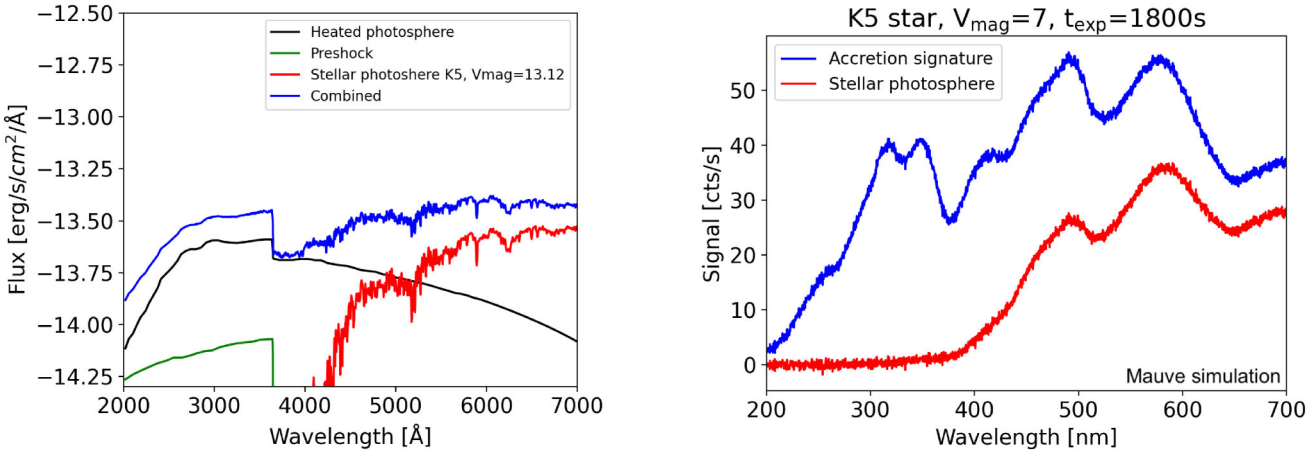

Figure 16. Left: SED of a pre-main sequence star at $V_{\rm mag}$=13.12 displaying accretion (blue line) which includes contributions from the pre-shock (green line), heated photosphere–post-shock (black line) and stellar photosphere (red line). Figure reproduced from L. Hartmann et al. (2016). Right: Mauve simulated data for the accreting model versus the non-accreting (quiet) photosphere for a brighter K5 star.

to Mauve. Mauve$^+$ will have a larger telescope and higher spectral resolving power to resolve single spectral lines. Mauve$^+$'s preliminary design includes a 25+ cm telescope coupled with a spectrograph ($R \approx 1000$) covering 180–500 nm. These characteristics will allow to use this space telescope to investigate the high-energy environments of exoplanet host stars, monitor accretion processes, and stellar flaring and provide critical UV coverage for transient multimessenger events, with the capability of resolving individual spectral lines.

ACKNOWLEDGEMENTS

The Mauve project has received funding from the European Union's Horizon Europe research and innovation programme under grant agreement No. 101082738. TAAS is grateful for support from the Fredrick Hunt Physics and Astronomy Fund and the Natural Sciences and Engineering Research Council of Canada (NSERC) through the Discovery Grant program. CD acknowledges support from NASA grant No. 80NSSC23K1115, the Alfred P. Sloan Research Fellowship, and the IBM Einstein Fellow Fund at theInstitute for Advanced Study, Princeton. EP and SR are co-funded by the European Union (ERC-2022-AdG, 'StarDance: the non-canonical evolution of stars in clusters', Grant Agreement 101093572, PI: EP). KV's research is funded by the Hungarian National Research, Development and Innovation Office grant Élvonal KKP-143986.

Authors' contributions: The Mauve Science Team has prepared this group publication to show the range of interests of the survey collaboration. While the survey programme is a collaborative initiative, and members are involved in multiple science themes, each member contributed to the publication as follows:

(i) Radiation mechanisms of stellar flares on M-dwarfs and young Sun-like stars: HM and KN.
(ii) Probing coronal mass ejections through UV dimming signatures: CD and HL.
(iii) Quiescent UV emission in low-mass stars: MAA, AN, and KV.
(iv) Young exoplanet hosts and HWO: GMD and KGS.
(v) The Classical Be star survey: TAAS and AR.
(vi) Accretion variability of Herbig Ae/Be stars and implications for planet formation: CMJK and DD.
(vii) Do Herbig Ae/Be stars exhibit dipper and burster behaviour: ETW, JJS, and PFF.
(viii) Binaries in exotic stellar populations: EP and SR.

CONFLICT OF INTEREST

GT, MT, and JT are Directors of Blue Skies Space Ltd; BJW, SR, AS, and IS are employees of Blue Skies Space Ltd. The other authors declare no conflict of interest.

DATA AVAILABILITY

All data for this paper are contained within the article; BSSL is able to share simulated data upon request.

REFERENCES

Agüeros M. A. et al., 2011, ApJ, 740, 110
Agüeros M. A. et al., 2018, ApJ, 862, 33
Airapetian V. S., Glocer A., Gronoff G., Hébrard E., Danchi W., 2016, Nat. Geosci., 9, 452
Andrews S. M. et al., 2018, ApJ, 869, L41
Anusha R., Sigut T. A. A., 2025, ApJ, 988, 129
Anusha R. et al., 2021, MNRAS, 501, 5927
Archer R. et al., 2020, Nat. Astron., 4, 1017
Balona L. A., Ozuyar D., 2021, ApJ, 921, 5
Birney M., Whelan E. T., Dougados C., Pascucci I., Murphy A., Flores-Rivera L., Flock M., Kirwan A., 2024, A&A, 692, L5
Boffin H. M. J., Carraro G., Beccari G., eds, 2015, Ecology of Blue Straggler Stars. Springer, Berlin, Heidelberg
Boggess A. et al., 1978, Nature, 275, 372
Bonito R. et al., 2023, ApJS, 265, 27
Brittain S. D., Kamp I., Meeus G., Oudmaijer R. D., Waters L. B. F. M., 2023, Space Sci. Rev., 219, 7
Calvet N., Gullbring E., 1998, ApJ, 509, 802
van Capelleveen R. F. et al., 2025, ApJ, 990, L8
Casey A. R. et al., 2019, ApJ, 880, 125
Chen H., Zhan Z., Youngblood A., Wolf E. T., Feinstein A. D., Horton D. E., 2021, Nat. Astron., 5, 298
Chen Y.-B., Lu H.-P., Tian H., Chen H.-C., Li Y., Yang Z.-H., Sun Z., Hou Z.-Y., 2025, ApJ, 987, L22
Cieza L. A. et al., 2016, Nature, 535, 258
Cody A. M. et al., 2014, AJ, 147, 82

Cody A. M., Hillenbrand L. A., David T. J., Carpenter J. M., Everett M. E., Howell S. B., 2017, ApJ, 836, 41
Cody A. M., Hillenbrand L. A., Chandragiri S., Morgan M., 2025, ApJ, 994, 253
Curtis J. L., Agüeros M. A., Mamajek E. E., Wright J. T., Cummings J. D., 2019a, AJ, 158, 77
Curtis J. L., Agüeros M. A., Douglas S. T., Meibom S., 2019b, ApJ, 879, 49
Curtis J. L. et al., 2020, ApJ, 904, 140
Das I., Vorobyov E., Basu S., 2025, ApJ, 983, 163
Dawson H. et al., 2024, A&A, 686, A25
Douglas S. T. et al., 2014, ApJ, 795, 161
Doyle J. G., Collier Cameron A., 1990, MNRAS, 244, 291
Empey A., Garcia Lopez R., Natta A., Manara C. F., Benisty M., Claes R., McGinnis P., 2025, A&A, 704, A10
Espinosa Lara F., Rieutord M., 2011, A&A, 533, A43
Fairlamb J. R., Oudmaijer R. D., Mendigutía I., Ilee J. D., van den Ancker M. E., 2015, MNRAS, 453, 976
Feinstein A. D., Seligman D. Z., France K., Gagné J., Kowalski A., 2024, AJ, 168, 60
Findeisen K., Hillenbrand L., Soderblom D., 2011, AJ, 142, 23
Fischer W. J., Hillenbrand L. A., Herczeg G. J., Johnstone D., Kospal A., Dunham M. M., 2023, in Inutsuka S., Aikawa Y., Muto T., Tomida K., Tamura M., eds, ASP Conf. Ser. Vol. 534, Protostars and Planets VII. Astron. Soc. Pac., San Francisco, p. 355
Fitzpatrick E. L., 1999, PASP, 111, 63
Flores C., Connelley M. S., Reipurth B., Duchêne G., 2022, ApJ, 925, 21
France K. et al., 2016, ApJ, 820, 89
Geller A. M. et al., 2017, ApJ, 840, 66
Gosnell N. M., Mathieu R. D., Geller A. M., Sills A., Leigh N., Knigge C., 2014, ApJ, 783, L8
Gosnell N. M., Mathieu R. D., Geller A. M., Sills A., Leigh N., Knigge C., 2015, ApJ, 814, 163
Gosnell N. M., Leiner E. M., Mathieu R. D., Geller A. M., Knigge C., Sills A., Leigh N. W. C., 2019, ApJ, 885, 45
Gray D. F., 2021, The Observation and Analysis of Stellar Photospheres. Cambridge Univ. Press, Cambridge
Gregory S. G., Donati J. F., 2011, Astron. Nachr., 332, 1027
Hartmann L., Herczeg G., Calvet N., 2016, ARA&A, 54, 135
Hastings B., Langer N., Wang C., Schootemeijer A., Milone A. P., 2021, A&A, 653, A144
Hauschildt P. H., 1993, J. Quant. Spec. Radiat. Transfer, 50, 301
Hawley S. L., Pettersen B. R., 1991, ApJ, 378, 725
Heber U., 2009, ARA&A, 47, 211
Heber U., 2016, PASP, 128, 082001
Heinzel P., 2024, MNRAS, 532, L56
Hills J. G., Day C. A., 1976, Astrophys. Lett., 17, 87
Howard W. S. et al., 2020, ApJ, 902, 115
Iben I., Jr, Tutukov A. V., 1999, in Solheim S. E., Meistas E. G., eds, ASP Conf. Ser. 169, 11th European Workshop on White Dwarfs. Astron. Soc. Pac., San Francisco, p. 432
Ikuta K., Namekata K., Notsu Y., Maehara H., Okamoto S., Honda S., Nogami D., Shibata K., 2023, ApJ, 948, 64
Isella A. et al., 2018, ApJ, 869, L49
Jiang Y., Chen H., Shen Y., Yang L., Li K., 2007, Sol. Phys., 240, 77
Johns-Krull C. M., 2007, ApJ, 664, 975
Kay C., Opher M., Kornbleuth M., 2016, ApJ, 826, 195
Kilpua E., Koskinen H. E. J., Pulkkinen T. I., 2017, Living Rev. Sol. Phys., 14, 5
Kippenhahn R., Weigert A., 1967, Z. Astrophys., 65, 251
Kirwan A., Murphy A., Schneider P. C., Whelan E. T., Dougados C., Eislöffel J., 2022, A&A, 663, A30
Koutoulaki M. et al., 2019, A&A, 625, A49
Kowalski A. F., Hawley S. L., Wisniewski J. P., Osten R. A., Hilton E. J., Holtzman J. A., Schmidt S. J., Davenport J. R. A., 2013, ApJS, 207, 15
Kowalski A. F., Allred J. C., Carlsson M., 2024, ApJ, 969, 121
Kumar A. et al., 2012, in Takahashi T., Murray S. S., den Herder J.-W. A., eds, Proc. SPIE Conf. Ser. Vol. 8443, Space Telescopes and Instrumentation 2012: Ultraviolet to Gamma Ray. SPIE, Bellingham, 84431N
Lauterborn D., 1970, A&A, 7, 150
Loyd R. O. P. et al., 2022, ApJ, 936, 170
Maehara H. et al., 2012, Nature, 485, 478
Mamajek E., Stapelfeldt K., 2024, preprint (arXiv:2402.12414)
Mason J. P., Woods T. N., Caspi A., Thompson B. J., Hock R. A., 2014, ApJ, 789, 61
Mathieu R. D., Geller A. M., 2009, Nature, 462, 1032
McCrea W. H., 1964, MNRAS, 128, 147
Mendigutía I., Eiroa C., Montesinos B., Mora A., Oudmaijer R. D., Merín B., Meeus G., 2011, A&A, 529, A34
Namekata K. et al., 2017, ApJ, 851, 91
Namekata K. et al., 2020, PASJ, 72, 68
Namekata K. et al., 2021, Nat. Astron., 6, 241
Namekata K., Maehara H., Notsu Y., Honda S., Ikuta K., Nogami D., Shibata K., 2025, ApJ, 993, 80
Núñez A., Agüeros M. A., 2016, ApJ, 830, 44
Núñez A. et al., 2015, ApJ, 809, 161
Núñez A., Agüeros M. A., Covey K. R., López-Morales M., 2017, ApJ, 834, 176
Núñez A. et al., 2022, ApJ, 931, 45
Núñez A. et al., 2024, ApJ, 962, 12
Panthi A., Subramaniam A., Vaidya K., Jadhav V., Rani S., Thirupathi S., Pandey S., 2023, MNRAS, 525, 1311
Pascucci I., Cabrit S., Edwards S., Gorti U., Gressel O., Suzuki T. K., 2023, in Inutsuka S., Aikawa Y., Muto T., Tomida K., Tamura M., eds, ASP Conf. Ser. Vol. 534, Protostars and Planets VII. Astron. Soc. Pac., San Francisco, p. 567
Pascucci I. et al., 2025, Nat. Astron., 9, 81
Perets H. B., Fabrycky D. C., 2009, ApJ, 697, 1048
Petrov P. P., Gahm G. F., Djupvik A. A., Babina E. V., Artemenko S. A., Grankin K. N., 2015, A&A, 577, A73
Pineda J. S., Youngblood A., France K., 2021, ApJ, 911, 111
Pinte C., Teague R., Flaherty K., Hall C., Facchini S., Casassus S., 2023, in Inutsuka S., Aikawa Y., Muto T., Tomida K., Tamura M., eds, ASP Conf. Ser. Vol. 534, Protostars and Planets VII. Astron. Soc. Pac., San Francisco, p. 645
Porter J. M., Rivinius T., 2003, PASP, 115, 1153
Rebull L. M., Stauffer J. R., Cody A. M., Hillenbrand L. A., Bouvier J., Roggero N., David T. J., 2020, AJ, 159, 273
Reiter M. et al., 2018, ApJ, 852, 5
Richey-Yowell T., Shkolnik E. L., Schneider A. C., Osby E., Barman T., Meadows V. S., 2019, ApJ, 872, 17
Rivinius T., Baade D., Štefl S., 2003, A&A, 411, 229
Rivinius T., Carciofi A. C., Martayan C., 2013, A&AR, 21, 69
V. Réville V., Brun A. S., Matt S. P., Strugarek A., Pinto R. F., 2015, ApJ, 798, 116
Saba A., Favata F., Savini G., Tinetti G., Bradley L., Stotesbury I., Tessenyi M., 2025, RAS Techn. Instrum., 4, rzaf045
Sackmann I. J., Boothroyd A. I., 1999, ApJ, 510, 217
Schneider A. C., Shkolnik E. L., 2018, AJ, 155, 122
Shibata K., Magara T., 2011, Living Rev. Sol. Phys., 8, 6
Shkolnik E. L., Barman T. S., 2014, AJ, 148, 64
Sigut T. A. A., 2018, in Mendoza C., Turck-Chièze S., Colgan J., eds, ASP Conf. Ser, Vol. 515, Workshop on Astrophysical Opacities. Astron. Soc. Pac., San Francisco, p. 213
Sigut T. A. A., Ghafourian N. R., 2023, ApJ, 948, 34
Sigut T. A. A., Jones C. E., 2007, ApJ, 668, 481
Simões P. J. A., Araújo A., Válio A., Fletcher L., 2024, MNRAS, 528, 2562
Sindhu N., Subramaniam A., Radha C. A., 2018, MNRAS, 481, 226
Sindhu N. et al., 2019, ApJ, 882, 43
Skumanich A., 1972, ApJ, 171, 565
Stapper L. M., Hogerheijde M. R., van Dishoeck E. F., Mentel R., 2022, A&A, 658, A112
Stelzer B., Marino A., Micela G., López-Santiago J., Liefke C., 2013, MNRAS, 431, 2063
Stelzer B., Damasso M., Scholz A., Matt S. P., 2016, MNRAS, 463, 1844
Struve O., 1931, ApJ, 73, 94
Townsend R. H. D., Owocki S. P., Howarth I. D., 2004, MNRAS, 350, 189

Valenti J. A., Basri G., Johns C. M., 1993, AJ, 106, 2024
Veronig A. M. et al., 2025, Living Rev. Sol. Phys., 22, 2
Wallerstein G., Sneden C., 1982, ApJ, 255, 577
Waters L. B. F. M., Waelkens C., 1998, ARA&A, 36, 233
Whelan E. T. et al., 2014, A&A, 565, A80
Williams J. P., Cieza L. A., 2011, ARA&A, 49, 67
Wilson D. J. et al., 2025, ApJ, 978, 85
Xu Y., Tian H., Veronig A. M., Dissauer K., 2024, ApJ, 970, 60
Youngblood A. et al., 2021, Essential Ultraviolet Stellar Characterization for Cycle 1 JWST Transiting Planet Targets, HST Proposal. Cycle 29, ID. #16701
von Zeipel H., 1924, MNRAS, 84, 665
Zorec J., Briot D., 1997, A&A, 318, 443
Zorec J. et al., 2016, A&A, 595, A132

This paper has been typeset from a TEX/LATEX file prepared by the author.